HHS Public Access

Author manuscript

Neurobiol Dis. Author manuscript; available in PMC 2020 June 01.

Published in final edited form as:

Neurobiol Dis. 2020 June ; 139: 104786. doi:10.1016/j.nbd.2020.104786.

Dysregulated iron metabolism in *C. elegans catp-6/ATP13A2* mutant impairs mitochondrial function

Nikhita Anand[1], **Angelina Holcom**[1], **Michael Broussalian**[1], **Minna Schmidt**[1], **Shankar J. Chinta**[1,2], **Gordon J. Lithgow**[1], **Julie K. Andersen**[1,#], **Manish Chamoli**[1,#]

[1]Buck Institute for Research on Aging, 8001 Redwood Blvd., Novato, CA USA

[2]Touro University California,Vallejo USA

Abstract

Mutations in the human *ATP13A2* gene are associated with an early-onset form of Parkinson's disease (PD) known as Kufor Rakeb Syndrome (KRS). Patients with KRS show increased iron deposition in the basal ganglia, suggesting iron toxicity-induced neurodegeneration as a potential pathogenesis associated with the *ATP13A2* mutation. Previously we demonstrated that functional losses of ATP13A2 disrupt the lysosome's ability to store excess iron, leading to reduce survival of dopaminergic neuronal cells. To understand the possible mechanisms involved, we studied a *Caenorhabditis elegans* mutant defective in *catp-6* function, an ortholog of human *ATP13A2* gene. Here we show that *catp-6* mutant worms have defective autophagy and lysosomal function, demonstrate characteristic PD phenotypes including reduced motor function and dysregulated iron metabolism. Additionally, these mutants have defective mitochondrial health, which is rescuable *via* iron chelation or mitophagy induction.

Keywords

ATP13A2; *catp-6*; *lysosomes*; *iron metabolism*; *mitochondrial function*; *urolithin A*; iron chelation; *TFEB, Parkinson's disease*; *C. elegans*

Introduction

Parkinson's disease is a progressive neurodegenerative disorder for which etiology and pathogenesis is still incompletely understood. Over the last several years, many genes associated with autosomal recessive forms of Parkinsonism including *parkin* (*PARK2*), *DJ-1*

[#]Correspondance: MChamoli@buckinstitute.org, JAndersen@buckinstitute.org.

Author contributions:

MC and JKA conceptualized the project. MC designed experiments. NA and MC performed majority experiments. AH helped in collecting data for Fig. 3D and 3E. MB helped in collecting data for Fig. 1 and S1D. MS helped in collecting data for Fig 3A. MC wrote original manuscript draft with help from NA. SJC, GJL and JKA edited it. All authors discussed the results and contributed to the final manuscript.

(*PARK7*), *PINK1* (*PARK6*) and *ATP13A2* (*PARK9*) have been identified (Kitada *et al.* 1998; Bonifati *et al.* 2003; Valente *et al.* 2004; Ramirez *et al.* 2006). Genetic changes associated with homozygous or compound heterozygous mutations in the *ATP13A2* gene have specifically been shown to result in a rare juvenile form of PD, Kufor Rakeb Syndrome (KRS)(Behrens *et al.* 2010). The disease is partially responsive to L-DOPA therapy and is characterized by features including pyramidal signs, supranuclear gaze palsy, dystonia and dementia (Najim al-Din *et al.* 1994; Hampshire *et al.* 2001; Williams *et al.* 2005).

The *ATP13A2* gene encodes a lysosomal transmembrane type 5 ATPase pump that maintains lysosomal function (Ramirez *et al.* 2006; Dehay *et al.* 2012; Usenovic *et al.* 2012). In lysosomes, ATP13A2 has been suggested to function as an ATP-dependent cation transporter, although this has not been directly demonstrated (Ramirez *et al.* 2006). Deletion of the yeast ortholog of *ATP13A2*, ypk9 has been shown to increase sensitivity to heavy metals including cadmium, manganese, selenium and nickel, suggesting a critical role for ATP13A2 in the transport and regulation of these metals (Gitler *et al.* 2009; Schmidt *et al.* 2009). Previous work from our own laboratory demonstrated that functional losses in ATP13A2 disrupt the lysosome's ability to store excess iron, eventually leading to reduce survival of dopaminergic neuronal cells (Rajagopalan *et al.* 2016).

Since neurons are heavily dependent on mitochondria for their function, we asked whether dysregulated iron homeostasis resulting from ATP13A2 loss affects mitochondrial function. We studied this in a *C.elegans catp-6* mutant, which lacks an ortholog of the human *ATP13A2* gene. We show that similar to human *ATP13A2*, *catp-6* loss of function affects lysosomal function, and plays an important role in the maintenance of both iron homeostasis and mitochondrial function. Therapeutically, we show that iron chelation or compounds that induce mitophagy can rescue mitochondrial pathologies associated with ATP13A2 loss of function.

Materials and Methods

Caenorhabditis elegans strains and maintenance

C. elegans strains used in the study are: N2 (Bristol), RB2510 *W08D2.5(ok3473) IV* and NL5901 (*pkIs2386 [unc-54p::alphasynuclein::YFP + unc-119(+)]*). The strains were obtained from the *Caenorhabditis* Genetics Center (CGC), University of Minnesota, MN, USA. The allele *ok3473* is a knockout for *W08D2.5/catp-6* gene with an estimated deletion size of 900 bp as reported by CGC. The deletion results in a significant loss in *catp-6* mRNA and protein levels (Figure 1A,B and C).

C. elegans strains were maintained at 20°C under standard laboratory conditions as described previously (Stiernagle 2006). Worm populations were maintained in 60 mm NGM agar plates (3 g/L NaCl, 17 g/L agar; 2.5 g/L peptone; 1 mM $CaCl_2$, 5 mg/L cholesterol, 1 mM $MgSO_4$, 25 mM KPO_4) seeded with OP50 *Escherichia coli*. During experiments synchronized population of worms were obtained by a 2-hour egg-lay from day-1 adult hermaphrodites on *E. coli* OP50 seeded 60 mm NGM agar plates. Post 2-hour adults were removed and the eggs were left to develop into adults at 20°C.

Compound preparation and treatment

A 100 mM stock of Urolithin A (UA) (sc-475514) and TFEB enhancer was prepared in sterile DMSO (Sigma) and stored in small aliquots at −20°C. From the stock solution, 130 μL of the working solution (50 μM UA or TFEB enhancer) was prepared by mixing 1.5 μL of stock solution (or DMSO only for control plates, 0.05% DMSO) with 128.5 μL of sterile water, and was added to the top of the 35 mm NGM plates (3 mL NGM agar) already seeded with a bacterial OP50 lawn. Stock solution of Calcium Disodium Ethylenediaminetetraacetic acid (CaEDTA) (Sigma) was prepared at 75 mM in sterile water and stored at 4°C. The 35 mm NGM plates (3 mL NGM agar) already seeded with a bacterial OP50 lawn was spotted with 100 μL of stock solution at a final concentration of 2.5 mM CaEDTA. Control plates for CaEDTA were treated with 100 μL of sterile water. Compound solution was distributed over the entire plate surface and allowed to dry in a sterile hood with lid open for at least 45 minutes in order to ensure complete drying of the agar/bacterial surface. We have seen that not doing so keeps the agar/bacterial surface moist, increasing the chances of worm loss from the moist edges of the plate. We chose to add compounds on top of the seeded plates and not in the agar plate to ensure maximum bioavailability and ensure stability of the compounds. Plates were then allowed to sit at 20°C for 24 hours before use or before moving into 4°C. Plates were stored for no longer than two weeks.

During experiments day-1 hermaphrodites were allowed to lay eggs for 2 hours on the non-compound treated plate. Equal number of synchronized eggs (35–40 per plate) were then picked with platinum pick and moved to a compound-treated plate and allowed to develop into adults at 20°C. Young day-1 adult worms were then used for the mitochondrial toxicity assay.

Mitochondrial toxicity assay

Mitochondrial toxin rotenone (complex I inhibitor) was used to assess the mitochondrial health. A 100 mM stock of rotenone was prepared in the sterile DMSO and stored in small aliquots at −20°C. From the stock solution, final working solution of rotenone (25 and 50 μM) was prepared in S-basal solution (5.85 g/L NaCl, 1g/L K_2HPO_4, 6 g/L KH_2PO_4, H2O to 1 L) and dispensed in a 96-well flat bottom plate (40 μL per well). All the wells including control wells were matched to consist 0.05%. Synchronized populations of day-1 adult worms (grown on control, CaEDTA, TFEB enhancer and UA) were picked and transferred to individual wells (10–15 worms per well). Three hours post-rotenone exposure, worms were scored dead or alive under the microscope. Worms that failed to display touch-provoked movement were scored as dead. Values represent percent survival ± SD.

Mounting worms and imaging

Microscopic slides containing pads of 2% agarose were prepared 30 minutes before mounting worms. Around 2–5 μL of 2 mM levamisole was pipetted out on the center of the agarose pads. Worms were transferred to the levamisole drop, and a cover slip was placed on top before imaging.

Adult lifespan assays

Plate preparation: A 450 mM stock solution of ferric ammonium citrate (FAC) (Sigma) was prepared in a sterile water. The 35 mm FuDR (Sigma) (10 μg/ml or 40.6 μM) containing NGM plates (3 mL NGM agar) already seeded with a bacterial OP50 lawn was spotted with FAC to make a final concentration of (15–50 mM) in sterile water. Control plates were treated with (9–30%) ammonium citrate (Sigma) as negative iron control. For zinc treated plates, 1 M stock solution of $ZnSo_4$ was prepared in sterile water and spotted at a final concentration of 500 μM. Plates were stored at 20°C overnight and then used for worms transfer or stored at 4°C for no longer than two weeks.

Age-synchronized day-1 worms (n=35 per plate) were then picked and transferred to FAC, zinc or control FuDR plates. Worms were transferred to fresh-compound treated plates every alternate day for 1st and 2nd week and then once a week. Worms were scored dead or alive every alternated day. Worms that failed to display touch-provoked movement were scored as dead. Worms that died from causes other than aging, such as sticking to the plate walls, internal hatching of eggs ('bagging'), or gonadal extrusion were censored. All lifespan experiments were performed at 20°C. Survival graphs were plotted using GraphPad Prism 8 (GraphPad Software, Inc., La Jolla, CA).

Thrashing assay for motor function

Egg-lay synchronized populations of N2, *catp-6(ok3473)* and (*pkIs2386 [unc-54p::alphasynuclein::YFP + unc-119(+)]*) worms were grown at 20°C. Thrashing rate was measured when worms reached reproductive adult stage. Thrashing was measured by recording a 30 second video of day-1 worms transferred to a sterile glass slide in a drop of S basal buffer. The worms were allowed to acclimate to the environment for 30 second and then video recorded under Leica stereomicroscope using corresponding software (30 second, n=30 in triplicate). For analysis, the video was slowed down and movement of the worm's head and/or tail to the same side was counted as one thrash. Worms which curled up or did not show any movement were not included in the analysis. Thrashing rate for the individual worm was plotted and average thrashing rate was determined.

RNA isolation and quantitative real-time polymerase chain reaction (qRT-PCR) of iron metabolism genes

RNA was isolated from 400–500 day-1 adult N2 and *catp-6(ok3473)* worms grown at 20°C. The worms were washed with 1X M9 buffer (g/L Na_2HPO_4, 3 g/L KH_2PO_4, 5 g/L NaOH, 1 mL/L of 1M MgSO4 solution) to get rid of any attached bacteria and finally collected in 300 μL of RNA lysis buffer supplied with a Zymogen RNA isolation kit. RNA was isolated according to the supplier protocol. The RNA concentration was quantified using NanoDrop 2000 Spectrophotometer. A total of 2000 ng RNA was subsequently reverse-transcribed to cDNA using iScript cDNA Synthesis Kit. Real time PCR was then performed using SYBR green master mix in a Light cycler 480II system. The relative gene expression was calculated by $2^{-\Delta\Delta Ct}$ method. The sequence of the qRT primers used for the analysis is provided in a Table 1 and were obtained from the previously published study (Lapierre *et al.* 2013; van den Ecker *et al.* 2015).

Mitochondrial membrane potential quantification using TMRM (tetramethylrhodamine)

TMRM plate preparation: From a stock solution of 100 μM TMRM (Thermo, T668) prepared in DMSO a final concentration of 150 nM TMRM (diluted in water) was added to the top of the 35 mm NGM plates (3 mL NGM agar) already seeded with a bacterial OP50 lawn. TMRM solution was distributed over the entire plate surface and allowed to dry in a sterile hood with lid open for at least 45 minutes in order to ensure complete drying of the agar/bacterial surface. Since TMRM is light-sensitive, plates were covered with aluminum foil and were allowed to sit at 20°C for 24 hours before use.

Egg-lay synchronized populations of N2 and *catp-6(ok3473)* worms were grown at 20°C. Late L3 larval stage worms were picked and transferred onto TMRM plates for 24 hours at 20°C and then transferred to non-TMRM plates for 1 hour to remove excess stain. As a positive control we transferred 20–30 N2 worms from the 24 hours TMRM treated N2 plate onto FCCP supplemented non-TMRM plate for 1 hour. About 20–30 worms per strain were picked and mounted on agarose pad as mentioned above for visualization of TMRM fluorescence under Zeiss Imager Z1 fluorescence microscope using rhodamine filters. Quantification of images was performed using NIH ImageJ software. We quantified the fluorescence intensity of the TMRM stain in the whole body for an individual worm and normalized it to the body size of the worm. Graph represents the average fluorescence intensity ± SD intensity of all the worms shown in the image.

LysoTracker Red staining

LysoTracker Red stain plate preparation: From a stock solution of 1 mM LysoTracker Red DND-99 (Molecular Probes) prepared in DMSO a final concentration of 100 nM stain (diluted in water) was added to the top of the 35 mm NGM plates (3 mL NGM agar) already seeded with a bacterial OP50 lawn. LysoTracker Red stain solution was distributed over the entire plate surface and allowed to dry in a sterile hood with lid open for at least 45 minutes in order to ensure complete drying of the agar/bacterial surface.

Egg-lay synchronized populations of N2 and *catp-6(ok3473)* worms were grown at 20°C. Larval L4 stage N2 and *catp-6(ok3473)* worms were picked and transferred onto LysoTracker Red stained plates for 24 hours at 20°C. Post-24 hours, worms were picked and washed in a fresh drop of 1X M9 buffer and mounted on 2% agarose pad slides for microscopic visualization as mentioned above. Worm images were taken in a Zeiss Imager Z1 fluorescence microscope using rhodamine filters. Image analysis was performed using Image J (NIH) software by measuring mean LysoTracker fluorescence of each worm normalized to it's body size. Graph represents mean fluorescence intensity ± SD of all the worms shown in the image.

Basal and maximum oxygen consumption rate (OCR)

Basal and maximum OCR was measured using Seahorse XF96 equipment (Seahorse Bioscience Inc., North Billerica, MA, USA). Egg-lay synchronized day-5 adult N2 and *catp-6(ok3473)* worms (~200 per strain, n=20 worms per well) were used for measuring the basal and maximum OCR according to previously described protocol (NG AND GRUBER 2019). On the day of the assay we washed animals three times with 1X M9 buffer in a 15

mL conical tube to get rid of any attached bacteria. We transferred ~20 animals to each well of a Seahorse XF24 Cell Culture Microplate with 200 μL of 1X M9 buffer. We first measured the basal respiration rate in every well, followed by injection of Carbonyl cyanide-p-trifluoromethoxyphenylhydrazone (FCCP) (Cayman) in the wells to uncouple mitochondria.

We injected sodium azide at the end of the assay in every well to completely block mitochondrial respiration. These compounds were prepared in the final solution of 1X M9 buffer and were injected from the reagent ports automatically to the wells at the time indicated. All respiration parameters were normalized to the number of animals per well. Bar graph represents the average basal and maximum OCR ± SD.

Worm protein extraction, SDS-PAGE and Immunoblotting

Synchronized day-1 adult N2 and *catp-6* mutant worms were grown at 20°C. 400 worms per sample were collected in 1X M9 buffer. Worms were washed twice and suspended in RIPA lysis buffer supplemented with complete EDTA-free protease inhibitor cocktail (ROCHE). Worm pellets were sonicated for 15 cycles at maximum intensity in Bioruptor sonicator (Diagenode). Lysate was centrifuged at 1000 × g for 1 minute and clear protein lysate was transferred to fresh eppendorf. After protein estimation equal amount of protein was used for immunoblotting. Polyacrylamide gels (10%−15%) were used for the separation of proteins. 35 μg of total proteins were transferred to 0.2 μm nitrocellulose membranes using the BioRad blotting system. All membranes were blocked with blocking buffer. Primary antibodies γ-Tubulin (T1450), ATP13A2 (LS-B11104), cathepsin D Antibody (C-20) (sc-6486), LC3B Antibody (CST #2775) were used for immunoblotting of total proteins. Goat anti-rabbit-IgG-HRP (CST, 7074), horse anti-mouse IgG-HRP (CST, 7076) were used as secondary antibody in all immunoblotting experiments. Chemiluminescence intensities were detected with ChemiDoc imaging system (BioRad) and quantified using Image J software (NIH). γ-tubulin levels were used to normalize the intensities of bands.

Statistical analysis

Survival graphs were plotted using GraphPad Prism 8 (GraphPad Software, Inc., La Jolla, CA). All the statistical analysis of survival curve *P*-values was performed using the Log-rank (Mantel-Cox) test through the online software OASIS (http://sbi.postech.ac.kr/oasis). The *p*-values for the quantification of the immunoblot band intesnity, LysosTracker Red stain assay were determined using unpaired Student's test. The *p*-values for the quantification of relative fold mRNA difference in Figure 1D and 2C were calculated using ordinary two-way ANOVA by Multiple t-tests with correction for multiple comparisons using the Holm-Sidak method. The *p*- value for thrashing rate and TRMRM staining assay were determined using ordinary one-way ANOVA and Tukey's multiple comparisons test. The The *p*-values for OCR assay in Figure 3E was determined using ordinary two-way ANOVA and Sidak's multiple comparison test. The *p*-values for rotenone toxicity assay were determined using ordinary two-way ANOVA and Tukey's multiple comparisons test. All the experiments were repeated at least twice. *p*-values were designated as: $*P < 0.05$, $**P<0.01$ and $***P<0.001$, $****P<0.0001$, ns-not significant

Results

Loss of *catp-6* affects autophagy and lysosomal function in *C. elegans*

The human *ATP13A2* gene shares close homology with the *C. elegans CATP* genes, with CATP-6 being the closest homolog (Figure S1A). Given the important role of *ATP13A2* in regulating lysosomal function, we asked whether loss of *catp-6* in *C. elegans* also affects lysosomal function or not. We used *catp-6(ok3473)* mutant and genotype confirmed an estimated deletion of 900 bp as reported by the CGC. Deletion results in a significant loss of *catp-6* mRNA (Figure 1A) and protein levels (Figure 1B, 1C). We assessed autophagy and lysosomal function in these mutants by quantifying protein levels of autophagosome (cleaved LGG-1/LC3-II) and lysosome specific aspartyl protease ASP-3/cathepsin D (CATD), respectively. We see protein level of cleaved LGG-1/LC3-II is significantly reduced in *catp-6* mutant, suggesting decreased autophagosomes in *catp-6* mutant (Figure 1B, 1D). This decrease in cleaved LGG-1/LC3-II level seems not to result from enhanced clearance of autophagosomes by lysosomes, but rather due to defect in early autophagosome formation, as lysosomal function is defective in this mutant. We tested lysosomal function by monitoring the level of premature (P-CATD) and mature (M-CATD) form of pH dependent lysosomal enzyme aspartyl protease ASP-3/CATD. We see that levels of P-CATD are significantly high in the *catp-6* mutants compared to wild type N2 worms, suggesting reduced conversion of P-CATD to M-CATD, which is directly dependent on the acidity of the lysosomes. In support, we see lysosomal pH of *catp-6* mutant worms is less acidic, as seen by significantly low LysosTracker Red staining when compared to wild type N2 worms (Figure 1F, 1G). LysosTracker Red is a pH dependent stain that stains lower in worms with inability to maintain acidic lysosome. Finally, we also see that *catp-6* mutant worms show significantly low mRNA expression of several key genes required for autophagy and lysosomal function (Figure 1H) (Lapierre *et al.* 2013). All together these results show that loss in *catp-6* affects autophagy and lysosomal function.

Reduced motor function and dysregulated iron metabolism in *catp-6* mutants

Mutations in the *ATP13A2* gene in humans results in parkinsonism-like phenotypes characterized by a loss of motor function, hence we first investigated whether *catp-6* mutant displayed any observable motor function defect. Indeed, we found that the thrashing rate (body bends) of *catp-6* mutant worms was significantly reduced compared to wild type N2 worms (*catp-6* vs N2, 21 vs 47 average thrashes per 30 seconds) (Figure 2A). As a control for thrashing assay we used NL5901 transgenic worms, which expresses human α-synuclein under control of muscle specific *unc-54* promoter cells and how motor function defect. As expected we see a significant motor function defects in NL5901 worms as their thrashing rate was significantly low (NL5901 vs N2, 16 vs 47 average thrashes per 30 seconds) (Figure 2A). We also observed a significant delay in the rate of development in *catp-6* mutants when compared to wild type N2 worms (Figure S1B).

We next asked whether *catp-6* mutant worms showed any signs of dysregulated iron metabolism. We observed several of the core genes required for metabolizing iron were significantly down-regulated in *catp-6* mutants compared to wild type N2 worms (Figure 2B). Interestingly, we also observed that *catp-6* mutant worms showed enhanced sensitivity

towards externally supplied iron, suggesting an inability to regulate iron. The magnitude of suppression of mean average lifespan upon exposure to 15 mM ferric ammonium citrate (FAC) was much higher in *catp-6* mutant worms 22% (p=0.0008), (*catp-6(ok3473)* FAC (15 mM) [9.04 ± 0.36] vs *catp-6(ok3473)* [11.64 ± 0.59], Mean average lifespan ± SEM) with no significant changes in mean average lifespan of wild type N2 worms at similar dose (N2 FAC (15 mM) [13.43 ± 0.58] vs N2 control [13.78 ± 0.44], Mean average lifespan ± SEM) (Figure 2C, S1C). We also tested the effects of zinc supplementation *on catp-6* mutant, which was recently shown to have altered zinc homeostasis (BAESLER *et al.* 2019). We see magnitude of mean average lifespan suppression upon exposure to zinc was significantly high in *catp-6* mutants (21.4% p=0.0004, zinc treated *catp-6* vs untreated *catp-6*, 10.17 ± 0.46 vs 12.94 ± 0.45, mean average lifespan ± SEM) compared to wild type N2 worms (9.0% p=0.02, zinc treated N2 vs untreated N2, 13.42 ± 0.43 vs 14.75 ± 0.59, mean average lifespan ± SEM) (Figure S1D).

Defective mitochondrial function in *catp-6* mutants

Defects in mitochondrial function underlie many neurodegenerative diseases, including PD. The *catp-6* mutants have previously been shown to have an enhanced neuronal loss upon expression of just a single copy α-synuclein, a protein associated with mitochondrial dysfunction (Cooper *et al.* 2018). The fact that mutation in *catp-6* gene is enough to enhance susceptibility towards neuronal loss suggest defect in key process or organelle effecting α-synuclein pathology. We, therefore, asked whether mutation in *catp-6* alone results in enhanced mitochondrial defects. A characteristic feature of defective mitochondria is that they are unable to maintain membrane potential. Using the membrane potential based fluorescent dye tetramethylrhodamine (TMRM), which fluoresces only in healthy mitochondria, we demonstrated that *catp-6* mutants show significantly lower TMRM fluorescence compared to wild type N2 worms (Figure 3A–B). As a positive control for the assay we exposed TMRM-stained N2 worms to the mitochondrial uncoupler FCCP (10 μM for 1 hour) known to reduce mitochondrial membrane potential. In addition, *catp-6* mutants displayed increased sensitivity to the mitochondrial toxin, rotenone (Figure 3C). Moreover, *catp-6* mutant worms displayed deficits in their maximum respiration capacity compared to wild type worms (Figure 3D–E). Taken together, these results suggest that *catp-6* mutant worms have multiple defects in mitochondrial function.

Iron chelation and mitophagy induction rescue mitochondrial defects in *catp-6* mutants

Next, we asked whether the observed defects in mitochondrial function could result from CATP-6 mediated dysregulation in iron metabolism. We used a known iron chelator Calcium Disodium Ethylenediaminetetraacetic acid (CaEDTA), which has been previously shown by our group to reduce iron levels and to increase lifespan in worms (Klang *et al.* 2014). We found that *catp-6* mutant worms treated with 2.5 mM CaEDTA showed significant protection against rotenone toxicity at lower concentration (25 μM) and showed a protective trend to a higher concentration of rotenone (50 μM), which was however not significant (Figure 4A). Significant protection against rotenone toxicity was also observed in *catp-6* mutants following treatment with a 50 μM dose of novel Transcription factor EB (TFEB) activator (recently discovered by our laboratory-not published) (Chamoli *et al.* 2017) and urolithin A (Ryu *et al.* 2016) both of which induce mitophagy in *C. elegans* (Figure 4B).

Discussion

ATP13A2 is a proton-pumping lysosomal ATPase whose mutation is associated with a rare juvenile onset form of PD known as KRS. ATP13A2 is highly expressed within dopaminergic Substantia Nigra pars compacta (DAergic SNpc) neurons and its expression has been reported to be decreased within DAergic SNpc neurons in post-mortem PD tissues and in the brains of patients with Lewy body disorder (LBD) (murphy *et al.* 2013). The physiological function of ATP13A2, and hence the role of its dysfunction in KRS and other related conditions, however remains elusive.

Lysosomes are principle reservoirs for chelatable iron (Kurz *et al.* 2004; KURZ *et al.* 2006; Kurz *et al.* 2008; Kurz *et al.* 2011; Terman AND Kurz 2013). Inhibition of vacuolar proton-pumping ATPase activity and subsequent increases in lysosomal pH have been reported to result in the release of chelatable ferrous iron from the lysosomes into the cytosol. Lysosomal pH has been reported to be compromised in *ATP13A2* mutant fibroblasts and in DAergic cell lines in which levels have been genetically reduced (Dehay *et al.* 2012). Interestingly, cytosolic iron levels have been reported to be elevated in the midbrain DAergic neurons of KRS patients.

The ATP13A2 transcript has been shown to contain a hypoxia response element (HRE) within its 5’ end, suggesting that its expression may be regulated by HIF1α. Transcription factor HIF1α is part of a highly conserved complex which serves to coordinately regulate a number of neuroprotective genes involved in cellular stress responses, including the maintenance of iron homeostasis and energy metabolism (Siddiq *et al.* 2005; Nakayama 2009; Greer *et al.* 2012). Previous work from our laboratory demonstrated expression of ATP13A2 within vulnerable midbrain DAergic neurons *in vivo* to be regulated by HIF1α signaling and knockdown of *ATP13A2* to inhibit HIF1α-mediated abrogation of cytosolic iron elevation and neurotoxicity in cultured dopaminergic DAergic cells under conditions of mitochondrial stress (Rajagopalan *et al.* 2016). These data suggest that ATP13A2 likely plays an important role in the maintenance of both cellular iron and mitochondrial homeostasis within these neurons.

Simialr to *ATP13A2*, loss in its *C. elegans* homolog *catp-6* has been previously identified as the modifier of human α-synuclein in a RNAi based screen of PD worm models (Hamamichi *et al.* 2008). Also, recently it was shown that *C. elegans catp-6* mutation predisposes worms towards α-synuclein induced sensitivity to various stresses including mitohcondrial stressor paraquat (Cooper *et al.* 2018). In order to explore the potential mechanistic link between losses in *ATP13A2*, iron and mitochondrial dysfunction, we studied *C. elegans catp-6* mutant. Our results show that, in conjunction with reductions in motility, *catp-6* mutant worms exhibit a reduction in iron regulation as indicated by alterated expression of several iron-metabolizing genes and increased sensitivity to exogenous iron exposure. Data showing *catp-6* mutants have defective lysosmal function suggest that alteration in iron homeostais in these mutant may result due to loss of chelatable iron from the lysosmes. Additionally, we also show defective mitochondrial function in these mutants as demonstrated by reduced mitochondrial membrane potential and maximal respiration rate as well as increased sensitivity to the mitochondrial toxin, rotenone. The latter was found to

be rescued via either iron chelation or induction of mitophagy (Figure 4). The ability of iron chelation to prevent rotenone sensitivity is of particular importance as it suggests that mitochondrial dysfunction in the *catp-6* mutants is causally linked to iron elevation. We hypothesize (Figure 5) that defective mitochondrial function in *catp-6*/*ATP13A2* mutants may be due to direct uptake of iron into mitochondria by the mitochondrial calcium uniporter (MCU-1), as has previously been reported in cultured hepatocytes (Uchiyama *et al.* 2008). Alternatively, role of *catp-6* in maintaining lysosmal function may effect the sorting nexin 3(Snx3)-retromer-mediated recycling of iron transporters and thus the iron homeostasis. This function of Snx3-retromer-mediated recycling of iron transporters is inhibited in dopamine neurons expressing α-synuclein which leads to neurodegeneration (Patel *et al.* 2018). This is in part why iron chelators has also been found effective in preventing α-synculein induced neurodegenration (Patel *et al.* 2018). The mitophagy inducer urolithin A is safe for humans and was reported to elicit improved mitochondrial health in a recent Phase-I clinical trial (Andreux *et al.* 2019). Interestingly, urolithin A is also a human gut metabolite which results from the transformation of ellagic acid (high in pomegranates) by the gut bacteria (Landete 2011). This raises the exciting possibility of the use of dietary interventions to treat *ATP13A2* loss-of-function in patients. Our findings, together with recent reports documenting a role for *catp-6* in maintaining Ca^{2+} (Narayanaswamy *et al.* 2019) and Zn^{2+} (Baesler *et al.* 2019) homeostasis also highlights the potential of using *catp-6* mutants as a platform for drug discovery and the identification of new genes regulating metal-induced toxicity.

Supplementary Material

Refer to Web version on PubMed Central for supplementary material.

Acknowledgments

This project was funded by NIH R21 grant NS0957 awarded to JKA. MC is supported by a postdoctoral fellowship from the Larry L. Hillblom Foundation. We thank Anand Rane and Dr. Dipa Bhaumik for help with laboratory resources. Strains were provided by the CGC, which is funded by NIH Office of Research Infrastructure Programs (P40 OD010440).

References

Andreux PA, Blanco-Bose W, Ryu D, Burdet F, Ibberson M et al., 2019 The mitophagy activator urolithin A is safe and induces a molecular signature of improved mitochondrial and cellular health in humans. Nature Metabolism 1: 595–603.

Baesler J, Kopp JF, Pohl G, Aschner M, Haase H et al., 2019 Zn homeostasis in genetic models of Parkinson's disease in Caenorhabditis elegans. J Trace Elem Med Biol 55: 44–49. [PubMed: 31345364]

Behrens MI, Bruggemann N, Chana P, Venegas P, Kagi M et al., 2010 Clinical spectrum of Kufor-Rakeb syndrome in the Chilean kindred with ATP13A2 mutations. Mov Disord 25: 1929–1937. [PubMed: 20683840]

Bonifati V, Rizzu P, van Baren MJ, Schaap O, Breedveld GJ et al., 2003 Mutations in the DJ-1 gene associated with autosomal recessive early-onset parkinsonism. Science 299: 256–259. [PubMed: 12446870]

Chamoli M, Chinta S, Schmidt M, Lithgow GJ and Andersen J, 2017 ROLE OF PHARMACOLOGICALLY INDUCED-TFEB IN AGING AND AGE-RELATED NEURODEGENERATION. Innovation in Aging 1: 1224–1224.

Cooper JF, Spielbauer KK, Senchuk MM, Nadarajan S, Colaiacovo MP et al., 2018 alpha-synuclein expression from a single copy transgene increases sensitivity to stress and accelerates neuronal loss in genetic models of Parkinson's disease. Exp Neurol 310: 58–69. [PubMed: 30194957]

Dehay B, Ramirez A, Martinez-Vicente M, Perier C, Canron MH et al., 2012 Loss of P-type ATPase ATP13A2/PARK9 function induces general lysosomal deficiency and leads to Parkinson disease neurodegeneration. Proc Natl Acad Sci U S A 109: 9611–9616. [PubMed: 22647602]

Gitler AD, Chesi A, Geddie ML, Strathearn KE, Hamamichi S et al., 2009 Alpha-synuclein is part of a diverse and highly conserved interaction network that includes PARK9 and manganese toxicity. Nat Genet 41: 308–315. [PubMed: 19182805]

Greer SN, Metcalf JL, Wang Y and Ohh M, 2012 The updated biology of hypoxia-inducible factor. EMBO J 31: 2448–2460. [PubMed: 22562152]

Hamamichi S, Rivas RN, Knight AL, Cao S, Caldwell KA et al., 2008 Hypothesis-based RNAi screening identifies neuroprotective genes in a Parkinson's disease model. Proc Natl Acad Sci U S A 105: 728–733. [PubMed: 18182484]

Hampshire DJ, Roberts E, Crow Y, Bond J, Mubaidin A et al., 2001 Kufor-Rakeb syndrome, pallido-pyramidal degeneration with supranuclear upgaze paresis and dementia, maps to 1p36. J Med Genet 38: 680–682. [PubMed: 11584046]

Kitada T, Asakawa S, Hattori N, Matsumine H, Yamamura Y et al., 1998 Mutations in the parkin gene cause autosomal recessive juvenile parkinsonism. Nature 392: 605–608. [PubMed: 9560156]

Klang IM, Schilling B, Sorensen DJ, Sahu AK, Kapahi P et al., 2014 Iron promotes protein insolubility and aging in C. elegans. Aging (Albany NY) 6: 975–991. [PubMed: 25554795]

Kurz T, Eaton JW and Brunk UT, 2011 The role of lysosomes in iron metabolism and recycling. Int J Biochem Cell Biol 43: 1686–1697. [PubMed: 21907822]

Kurz T, Gustafsson B and Brunk UT, 2006 Intralysosomal iron chelation protects against oxidative stress-induced cellular damage. FEBS J 273: 3106–3117. [PubMed: 16762036]

Kurz T, Leake A, Von Zglinicki T and Brunk UT, 2004 Relocalized redox-active lysosomal iron is an important mediator of oxidative-stress-induced DNA damage. Biochem J 378: 1039–1045. [PubMed: 14670081]

Kurz T, Terman A, Gustafsson B and Brunk UT, 2008 Lysosomes in iron metabolism, ageing and apoptosis. Histochem Cell Biol 129: 389–406. [PubMed: 18259769]

Landete JM, 2011 Ellagitannins, ellagic acid and their derived metabolites: A review about source, metabolism, functions and health. Food research international 2011 v.44 no.5: pp. 1150–1160.

Lapierre LR, De Magalhaes Filho CD, McQuary PR, Chu CC, Visvikis O et al., 2013 The TFEB orthologue HLH-30 regulates autophagy and modulates longevity in Caenorhabditis elegans. Nat Commun 4: 2267. [PubMed: 23925298]

Murphy KE, Cottle L, Gysbers AM, Cooper AA and Halliday GM, 2013 ATP13A2 (PARK9) protein levels are reduced in brain tissue of cases with Lewy bodies. Acta Neuropathol Commun 1: 11. [PubMed: 24252509]

Najim al-Din AS, Wriekat A, Mubaidin A, Dasouki M and Hiari M, 1994 Pallido-pyramidal degeneration, supranuclear upgaze paresis and dementia: Kufor-Rakeb syndrome. Acta Neurol Scand 89: 347–352. [PubMed: 8085432]

Nakayama K, 2009 Cellular signal transduction of the hypoxia response. J Biochem 146: 757–765. [PubMed: 19864435]

Narayanaswamy N, Chakraborty K, Saminathan A, Zeichner E, Leung K et al., 2019 A pH-correctable, DNA-based fluorescent reporter for organellar calcium. Nat Methods 16: 95–102. [PubMed: 30532082]

Ng LF, and Gruber J, 2019 Measurement of Respiration Rate in Live Caenorhabditis elegans. Bio-protocol 9: e3243.

Patel D, Xu C, Nagarajan S, Liu Z, Hemphill WO et al., 2018 Alpha-synuclein inhibits Snx3-retromer-mediated retrograde recycling of iron transporters in S. cerevisiae and C. elegans models of Parkinson's disease. Hum Mol Genet 27: 1514–1532. [PubMed: 29452354]

Rajagopalan S, Rane A, Chinta SJ and Andersen JK, 2016 Regulation of ATP13A2 via PHD2-HIF1alpha Signaling Is Critical for Cellular Iron Homeostasis: Implications for Parkinson's Disease. J Neurosci 36: 1086–1095. [PubMed: 26818499]

Ramirez A, Heimbach A, Grundemann J, Stiller B, Hampshire D et al., 2006 Hereditary parkinsonism with dementia is caused by mutations in ATP13A2, encoding a lysosomal type 5 P-type ATPase. Nat Genet 38: 1184–1191. [PubMed: 16964263]

Ryu D, Mouchiroud L, Andreux PA, Katsyuba E, Moullan N et al., 2016 Urolithin A induces mitophagy and prolongs lifespan in C. elegans and increases muscle function in rodents. Nat Med 22: 879–888. [PubMed: 27400265]

Schmidt K, Wolfe DM, Stiller B and Pearce DA, 2009 Cd2+, Mn2+, Ni2+ and Se2+ toxicity to Saccharomyces cerevisiae lacking YPK9p the orthologue of human ATP13A2. Biochem Biophys Res Commun 383: 198–202. [PubMed: 19345671]

Siddiq A, Ayoub IA, Chavez JC, Aminova L, Shah S et al., 2005 Hypoxia-inducible factor prolyl 4-hydroxylase inhibition. A target for neuroprotection in the central nervous system. J Biol Chem 280: 41732–41743. [PubMed: 16227210]

Stiernagle T, 2006 Maintenance of C. elegans. WormBook: 1–11.

Szklarczyk D, Franceschini A, Wyder S, Forslund K, Heller D et al., 2015 STRING v10: protein-protein interaction networks, integrated over the tree of life. Nucleic Acids Res 43: D447–452. [PubMed: 25352553]

Terman A, and Kurz T, 2013 Lysosomal iron, iron chelation, and cell death. Antioxid Redox Signal 18: 888–898. [PubMed: 22909065]

Uchiyama A, Kim JS, Kon K, Jaeschke H, Ikejima K et al., 2008 Translocation of iron from lysosomes into mitochondria is a key event during oxidative stress-induced hepatocellular injury. Hepatology 48: 1644–1654. [PubMed: 18846543]

Usenovic M, Tresse E, Mazzulli JR, Taylor JP and Krainc D, 2012 Deficiency of ATP13A2 leads to lysosomal dysfunction, alpha-synuclein accumulation, and neurotoxicity. J Neurosci 32: 4240–4246. [PubMed: 22442086]

Valente EM, Abou-Sleiman PM, Caputo V, Muqit MM, Harvey K et al., 2004 Hereditary early-onset Parkinson's disease caused by mutations in PINK1. Science 304: 1158–1160. [PubMed: 15087508]

van den Ecker D, Hoffmann M, Muting G, Maglioni S, Herebian D et al., 2015 Caenorhabditis elegans ATAD-3 modulates mitochondrial iron and heme homeostasis. Biochem Biophys Res Commun 467: 389–394. [PubMed: 26427876]

Williams DR, Hadeed A, al-Din AS, Wreikat AL and Lees AJ, 2005 Kufor Rakeb disease: autosomal recessive, levodopa-responsive parkinsonism with pyramidal degeneration, supranuclear gaze palsy, and dementia. Mov Disord 20: 1264–1271. [PubMed: 15986421]

Highlights

- Loss in *C. elegans catp-6* disrupts autophagy and lysosmal function
- CATP-6 mediates iron homesotais and mitochondrial function
- Iron chelation and mitophagy induction as potential therapeutic approach to resuce mitochondrial defects in *catp-6/ATP13A2* mutants

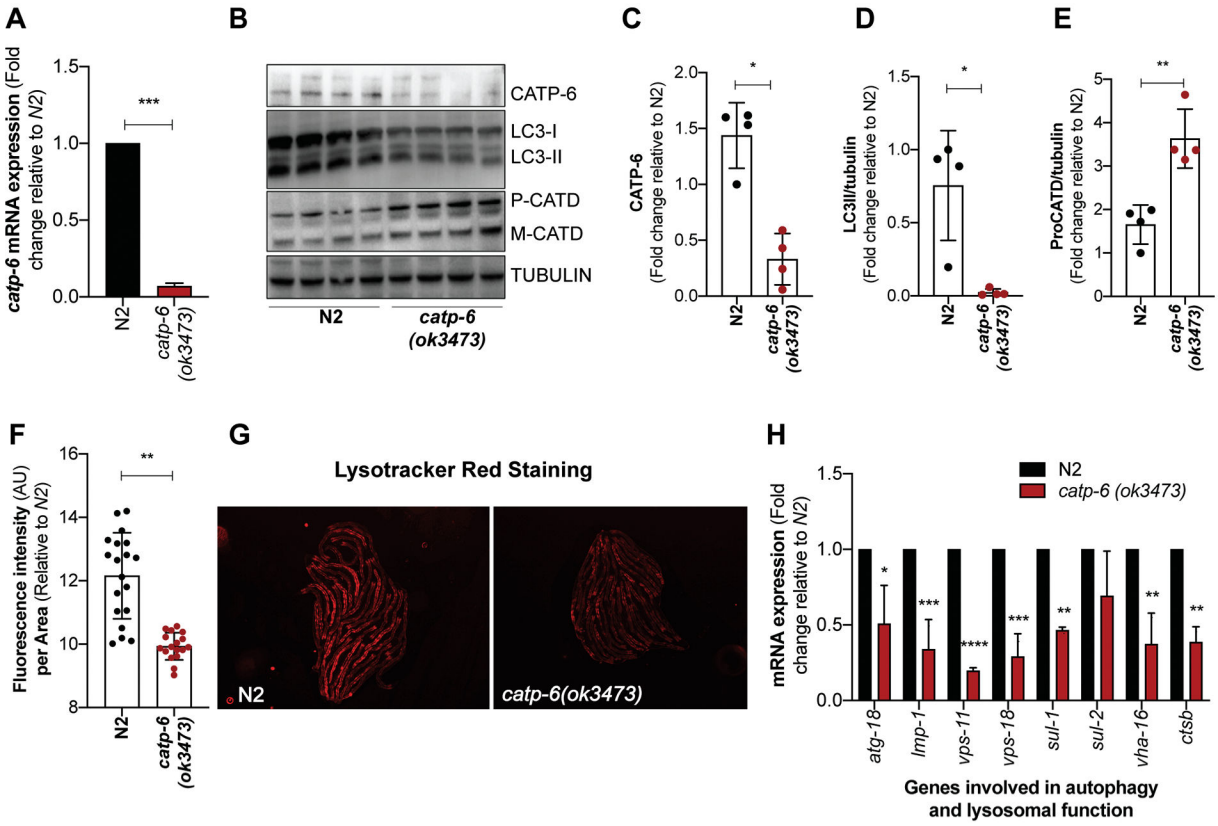

Figure 1: Loss of *catp-6* affects autophagy and lysosomal function in *C. elegans*.

(A) Graph represents fold change ± SD in the mRNA expression of *catp-6* in *catp-6(ok3473)* mutant relative to wild type N2 worms (n=2, *p*-values calculated using unpaired Student's t-test). **(B)** Immunoblot showing the level of CATP-6, autophagosome specific cleaved LGG-1/LC3-II protein and lysosome specific aspartyl protease ASP-3/cathepsin D (CATD) which exists as procathepsin D (P) and mature (M) cathepsin D and loading control γ-tubulin. **(C-E)** Graph represents the densitometric analysis of the bands, showing average band intensity ± SD of CATP-6, cleaved LGG-1/LC3-II and P-CATD normalized to loading control γ-tubulin (n=4, *p*-values calculated using unpaired Student's t-test) **(F)** Graph represents the mean fluorescence intensity ± SD of LysoTracker Red stain normalized to the body size for wild type N2 and *catp-6(ok3473)* worms. Quantification was performed on the whole body of an individual worm using NIH image J software (n=2, *p*-values calculated using unpaired Student's t-test). **(G)** Representative images of the N2 and *catp-6(ok3473)* worms showing LysoTracker red fluorescence. **(H)** Graph represents fold change ± SD in the mRNA expression of autophagy and lysosomal specific genes in *catp-6(ok3473)* mutant worms relative to wild type N2 worms (n=2, *p*-values calculated using ordinary two-way ANOVA by Multiple t-tests with correction for multiple comparisons using the Holm-Sidak method). All the *p*-values are represented as $*p < 0.05$, $**p<0.01$ $***p<0.001$ and $****p<0.0001$.

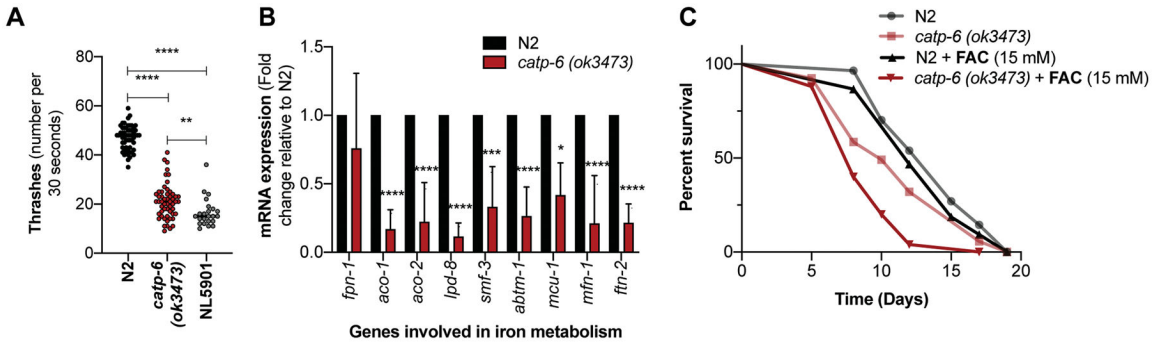

Figure 2: Reduced motor function and dysregulated iron metabolism in *catp-6* mutants.

(A) Quantification of the number of thrashes in N2 versus *catp-6(ok3473)* mutant worms. Graph represents average number of thrashes ± SD over the period of 30 seconds, where Individual dot represents single worm. NL5901 (*pkIs2386 [unc- 54p::alphasynuclein::YFP + unc-119(+)]* strain expressing human α-synuclein in muscles shows motor defects and served as a positive control for the assay. (n=3, *p*-values calculated using ordinary one-way ANOVA and Tukey's multiple comparisons test). **(B)** Graph represents fold change ± SD in the mRNA expression of iron-metabolizing genes in *catp-6(ok3473)* mutant worms relative to wild type N2 worms (n=5, *p*-values calculated using two-way ANOVA analysis). **(C)** The effect of ferric ammonium citrate (FAC) or ammonium citrate exposure as a negative control on survival of N2 and *catp-6(ok3473)* mutant worms. N2 control [13.78 ± 0.44] (median-14), N2 FAC (15 mM) [13.43 ± 0.58] (median-13), *catp-6(ok3473)* [11.64 ± 0.59] (median-11), and *catp-6(ok3473)* FAC (15 mM) [9.04 ± 0.36] (median-8). [Mean average lifespan ± SEM], (n=2, *p*-value calculated using Mantel-Cox Log rank test). All the *p*-values are represented as $*p < 0.05$, $**p<0.01$ and $***p<0.001$, $****p<0.0001$.

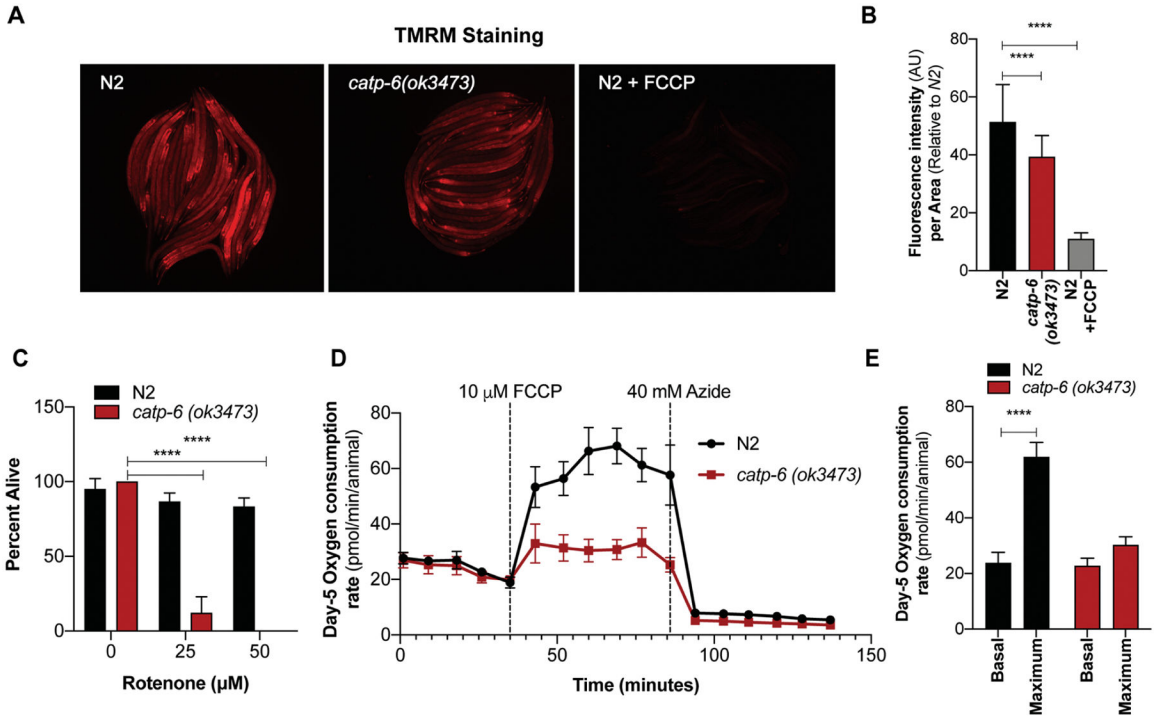

Figure 3: Defective mitochondrial function in *catp-6* mutants.

(A) Representative images of TMRM-stained N2, *catp-6(ok3473)* and TMRM-N2 worms exposed to 10 μM FCCP for 1 hour (positive control). **(B)** Graph represents the average mean fluorescence intensity ± SD of TMRM stain normalized to the body size. Quantification was performed on the whole body of an individual worm using NIH image J software (n=2, *p*-value calculated using ordinary one-way ANOVA and Tukey's multiple comparisons test). **(C)** Enhanced sensitivity of *catp-6(ok3473)* mutant worms to the mitochondrial toxin rotenone measured as percent survival ± SD (n=2, *p*-value calculated using ordinary two-way ANOVA and Tukey's multiple comparisons test). **(D-E)** Mitochondrial function in N2 and *catp-6(ok3473)* mutant worms as quantitated by oxygen consumption rate using the Seahorse. Bar graph represents average OCR consumption ± SD of day-5 N2 and *catp-6(ok3473)* worms (n=2, *p*-value calculated using ordinary two-way ANOVA and Sidak's multiple comparison test). All the *p*-values are represented as $*p < 0.05$, $**p<0.01$ and $***p<0.001$, $****p<0.0001$.

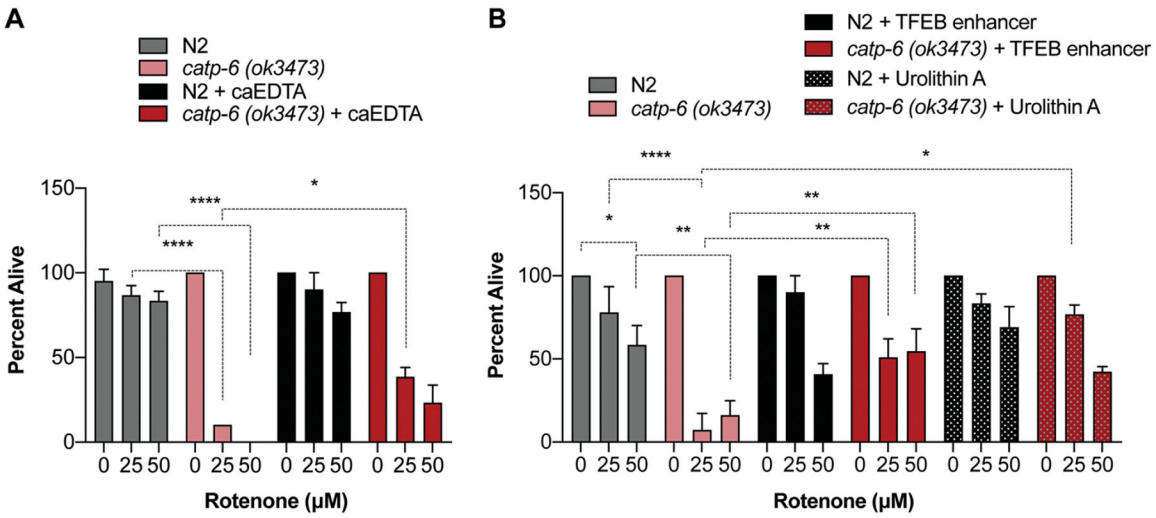

Figure 4: Iron chelation and mitophagy induction rescue sensitivity of *catp-6* to rotenone exposure.

Sensitivity of N2 and *catp-6(ok3473)* mutant worms to the mitochondrial toxin, rotenone, measured as percent survival ± SD in worms exposed to **(A)** the 2.5 mM iron chelator calcium-EDTA (Ca-EDTA) or **(B)** the 50 μM mitophagy-inducing agents (TFEB enhancer and urolithin A) throughout development (n=2, *p*-value calculated using ordinary two-way ANOVA and Tukey's multiple comparisons test). All the *p*-values are represented as **p* < 0.05, ***p*<0.01 and ****p*<0.001, *****p*<0.0001.

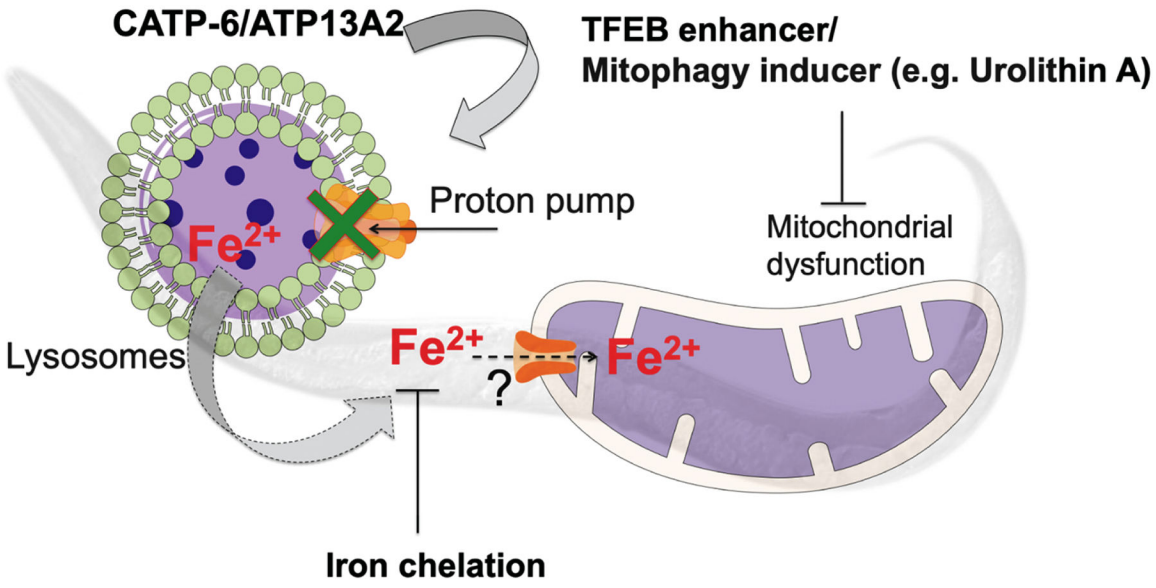

Figure 5: Schematic overview of the results.

The *catp-6*/*ATP13A2* gene encodes a lysosomal transmembrane type 5 ATPase pump that helps to maintain autophagy and lysosomal function. Loss in CATP-6 function results in dysregulated iron metabolism effecting mitochondrial function and rendering it sensitive to mitochondrial stress. Iron chelation, TFEB enhancement or mitophagy inductions all separately rescue sensitivity to the mitochondrial toxin, rotenone.

Table 1:

Sequence of the primers used in study

Gene	Primer	Sequence(5'−3')
catp-6	Forward	AAGTCTAACGCCACAATTCCCACCGA
	Reverse	CCAAAAGTGATCGACAAGGAAT
atg-18	Forward	AAATGGACATCGGCTCTTTG
	Reverse	TGATAGCATCGAACCATCCA
lmp-1	Forward	ATCCGCCACCGCTTCGCATT
	Reverse	TCGAGCTCCCACTCTTTGGCG
vps-11	Forward	TCCGCTTGTCGTCCTGGAGC
	Reverse	TCACACGCCGAGCACTTGGT
vps-18	Forward	CGAGCCGGCGCCAGTTGTAA
	Reverse	TCCATCCGGCGAAAGCCACG
sul-1	Forward	CAGGATGGGATGAGTGGCACG
	Reverse	GGGTCTTCTGGTCCATGCGGC
sul-2	Forward	ATGGCAGCAGAAGGCACCCG
	Reverse	GCCATTTTCCAACCATGCCAGTTGC
vha-16	Forward	AGGCGCTGACTCGCGGACTT
	Reverse	TGGTCTCTGGTGAAGAGTTCCGGTG
ctsb/cpr-1	Forward	CGCCAAGGACAAGCACTTCGGA
	Reverse	ACCTTGGCCTTTCCGGCGAC
fpn-1	Forward	GGACT CAAAGGCGTCAAGTT
	Reverse	TAGGATGCGGCGAGGTTAT
aco-1	Forward	GTCGTAGATCTTGCCGCTATG
	Reverse	GGCTTCAAGGTTTCCGTAGT
aco-2	Forward	TCACTCCTCTTCGTCCATCT
	Reverse	GGACGTTTCAATCTGTCTTTCAC
lpd-8	Forward	GCTTTGTACAAGCAGCTCGAT
	Reverse	CGCTGAGCTGAAATCGTATGTT
smf-3	Forward	CTCGTTTGGTACTGTGGATGTT
	Reverse	CAGAGAGGGATTACTCCGTTAGA
abtm-1	Forward	TCAGATCGCAGGCAGTTTAC
	Reverse	GTGAAAGCATGTCCTTGTGAATAC
mfn-1	Forward	CTTGCAGGCTAGGTATCGTTAT
	Reverse	TTGCAGGAACCTGGAATATGA
ftn-2	Forward	GTTAACAAGCAGATCAACATT
	Reverse	ACGCTCCTCATCCGATT
Genotype primers		
catp-6	outer primer-Forward	CTTAAAATTTCGCGGCTGAG
catp-6	outer primer-Reverse	TAAGGCCTTCCAAAAGAGCA

Gene	Primer	Sequence(5'−3')
catp-6	Inner primer-Forward	TTTTCGGCTTAGAAAACAGCA
catp-6	Inner primer-Reverse	TGGTGAGCTCGATGAATACG